Proceedings in Manufacturing Systems, Volume 17, Issue 2, 2022, 69-77 ISSN 2067-9238

QO-CARDSAT MICROSATELLITE CALCULATION METHODOLOGY OF THE POSITION OF THE JOINTS AND REQUIRED TORQUE TO OPEN THE PANELS

Dorel Florea ANANIA[1,*], Emilia BĂLAN[2], Miron ZAPCIU[3], Marilena STOICA[4], Andra Elena PENA[5]

[1, 2)] Assoc. Prof., PhD Eng., Robots and Production Systems Department, University "Politehnica" of Bucharest, Romania
[3)] Prof., PhD Eng., Robots and Production Systems Department, University "Politehnica" of Bucharest, Romania
[4)] Lecturer, PhD Eng., Department of Machine Elements and Tribology, University "Politehnica" of Bucharest, Romania
[5)] Lecturer, PhD Eng., Robots and Production Systems Department, University "Politehnica" of Bucharest, Romania

Abstract: *Microsatellites are the subject of many research projects addressed today in universities. The most successful microsatellites known are the CubeSats. An objective of this paper is to establish an optimal configuration of the structure of a microsatellite composed of several panels named Cardsat. A Cardsat is a thin panel-shaped satellite with low volume and weight. It is designed to perform the same functions as the CubeSat, but with a much smaller volume (up to 11 times smaller). In order to launch, the panels are folded and assembled by means of joints. They form a package. This paper presents a method for load calculation of a flexible structure QO-Cardsat used in microsatellite architecture for deploying into predefined configuration. The results presented in this article are the preliminary calculations necessary for the design of the actuation elements of the Cardsat type panels in a combined construction so that it is possible to open in the final configuration starting from the folded form required for the launch. The steps required for the technical design of the proposed panel configurations are: kinematic calculation to identify the position of the panels and their centers of mass for given angles, calculation of the resistant moments required to be overcome by the actuating elements of the spring type, calculation of springs (torsion/lamination). The calculation of the joint positions is carried out with the help of rotation matrices.*

Key words: *microsatellite, configuration, QO-Cardsat, matrix joints calculation, opening torque.*

1. INTRODUCTION

Microsatellites have been the focus of numerous research projects in recent years, being investigated both experimentally and numerically. The development of research methods allowed the constructive approach to microsatellites in order to manufacturing them quickly and cheaply. Typical microsatellite missions range from Earth observation, military domain, satellite service, amateur radio and on-orbit inspection to space exploration, which requires sophisticated launch and navigation control technology [1, 2].

One of the most successful microsatellites known today is the CubeSat, which is intended for low Earth orbit (LEO) to perform a number of scientific research functions and explore new space technologies. The smallest CubeSat (considered as a CubeSat unit = 1U) is a cube with a side length of 10 cm and a maximum weight of 1.33 kg. Today, 2U, 3U or 10U CubeSats are also being built. The specifications to develop the skills for design, manufacture and testing are standardizated today [19–22].

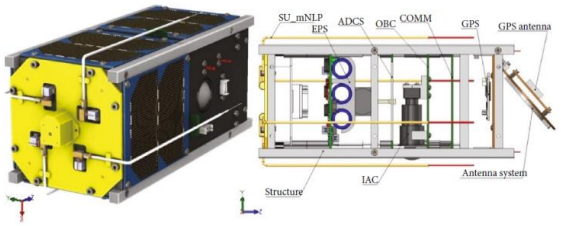

Fig. 1. CubeSat satellite structure [3].

A microsatellite is composed of a primary structure that supports the onboard payloads and secondary structures that enable the operation of the microsatellite and the data transmission (Fig. 1).

The structure of a CubeSats microsatellite consists of: EPS – electrical power subsystem, ADCS – attitude determination and control subsystem, OBC – on-board computer, COMM – communication subsystem, TT&C – telecommunications, tracking and command subsystem, ODCS – orbital determination and control subsystem, mechanical structure, payload, propulsion subsystem, thermal control subsystem, electronic components [1, 3].

Although CubeSat has achieved real success, it also has some disadvantages such as [19, 20]:

- though the size is relatively small, the specifications are still important (in the satellite field, every extra cubic centimeter or every gram to be placed in orbit has a negative impact on the cost);

[*] Corresponding author: Splaiul Independenței, 313, Sector 6, Bucharest, Romania,
Tel.: + 40 21-402 94 20;
E-mail addresses: *dorel.anania@upb.ro* (F.D. Anania), *emilia.balan@upb.ro* (E. Bălan), *miron.zapciu@upb.ro* (M. Zapciu), *marilena.stoica@upb.ro* (M. Stoica), *andra.pena@upb.ro* (A.E. Pena).

- while satellites with expandable solar panels have been developed, the solar collection system (via solar panels located outside the base) is not optimal.

The mechanical structure of the satellites weighs between 7% and 10% of the total mass of the satellite at launch. When defining design requirements two different areas must be considered [4]:

- internal requirements: are imposed by the mission and the interface with the component subsystems of the satellite;
- external requirements: are related to the satellite launch vehicle, its mission phases and the space environment in which the satellite and the instruments it carries will operate.

About 25% of satellite operational anomalies are actually due to the space environment affecting the control and management systems of the spacecraft and instruments. The low Earth orbit (LEO) space environment affects the performance and functionality of materials through phenomena such as atomic oxygen (AO), ultraviolet (UV) radiation, plasma, micrometeoroids and orbital debris (MMOD), as well as extreme thermal conditions due to temperature cycling dazzling [5].

The materials used in the space industry must show high performance, such as: a low degree of outgassing, high resistance to micro-cracking, dimensional stability (low coefficient of thermal expansion) during exposure to thermal cycles in space, resistance to ionizing radiation (α, β, X rays, but mainly UV/VUV and γ), upon attack with oxygen atoms, upon irradiation with protons and electrons [6].

Dimensional stability is crucial for various spacecraft structures, especially for parts that deal with precision, such as the antenna, the skeleton structure, and the optical support structure [7, 8].

The Cardsat microsatellite is a thin panel-shaped satellite with low volume and low weight that can maximize solar energy collected by the solar panel, thereby maximizing the ratio of solar exposure area to mass. It is designed to perform the same functions as the CubeSat, but with a much smaller volume (up to 11 times smaller).

The objectives of the presented paper are:

- establishing an optimal configuration of the structure of a microsatellite composed of several Cardsat panels; in folded state the structure of a Cardsat-type panel is similar to the structure of CubeSats-type microsatellites;
- establishing a design methodology for the actuation elements of the Cardsat type panels assembled in the form of a package, so that it is possible to open them in the desired configuration starting from the folded form required for launch.

2. LAUNCH CONDITIONS, ORBIT & RETURN

The design of space structural systems is dictated by mass, stiffness and strength requirements. On the one hand, stiffness is necessary to ensure the good behavior of the satellite, and on the other hand, by reducing the weight, it is possible to increase the payload, which expands the objectives of the mission, of the electronic load and, at the same time, reduces the launch cost. The structure design in terms of the material used as well as the mechanical parts of a satellite generally represents a large percentage of its mass. Therefore, it is important that the choice of the appropriate material and the structural configuration are conditioned by the minimization of the mass. Finally, the microsatellite concept is related to general constraints and requirements of stiffness and natural frequency [3].

Considering the mass, rigidity and strength requirements of the equipment, it is absolutely necessary to carry out specific design analyzes to establish the feasibility of using materials, either conventional materials such as aluminum alloy, or composite materials.

Currently, the Northrop Grumman Pegasus, JAXA Epsilon, and the Rocket Lab Electron rocket are the only operational small launch vehicles [9]. There are limited recovery options to retrieve test samples from orbit. ESA, Space Rider, the Soyuz capsule and the SpaceX Dragon capsule allow the option to retrieve samples from space, but are expensive to operate and have a limited flight frequency. Ground testing offers lower testing cost; however, the challenge of simulating the real space environment tends to decrease the accuracy of the results.

3. MICROSATELLITE CONFIGURATION STRUCTURE

One of the objectives of the work is to establish an optimal configuration of the structure of a microsatellite composed of several Cardsat panels. In order to launch, the panels are folded and assembled by means of joints. They form a panel package.

For a launch system specific to CubeSats type microsatellites, a maximum of 9 overlapping panels can be used in a package, with a distance of 1.25 mm between them. The dimensions of a folded microsatellite are L340.5 × H100 × W100 mm (Fig. 2). The space between the panels can be used for the assembly/construction of joints necessary for the controlled opening of the panels to achieve the desired configuration.

The preliminary dimensional conditions to be taken into account in the modeling/design/virtual prototyping phase are shown in Figs. 3–10.

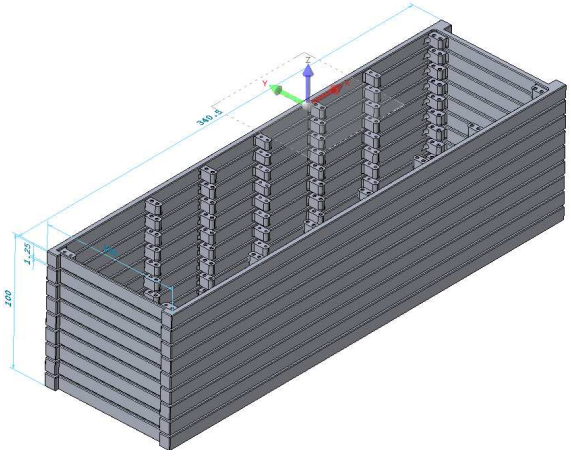

Fig. 2. Folded Cardsat package.

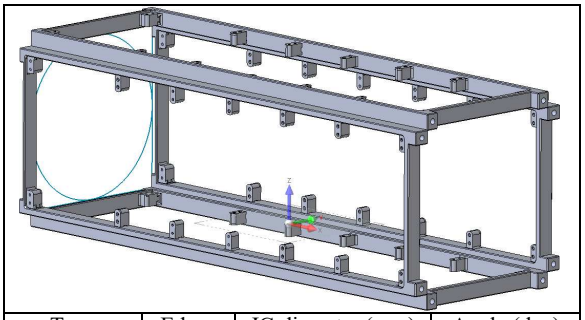

Type	Edges	IC diameter (mm)	Angle (deg)
Quadri	4	100	90

Fig. 3. Quadri unfolded.

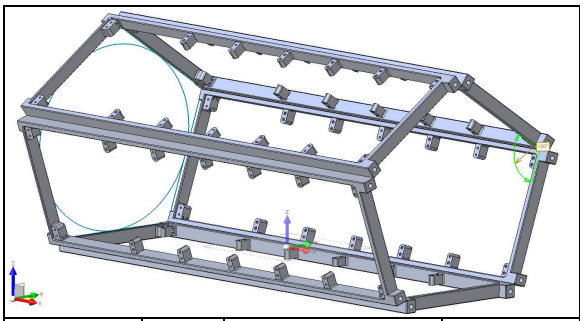

Type	Edges	IC diameter (mm)	Angle (deg)
Penta	5	137.64	108

Fig. 4. Penta unfolded.

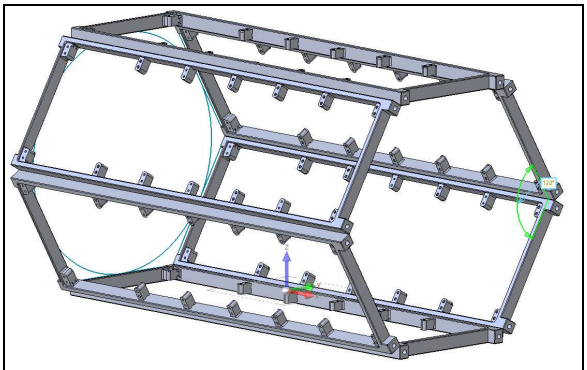

Type	Edges	IC diameter (mm)	Angle (deg)
Hexa	6	173.21	120

Fig. 5. Hexa unfolded.

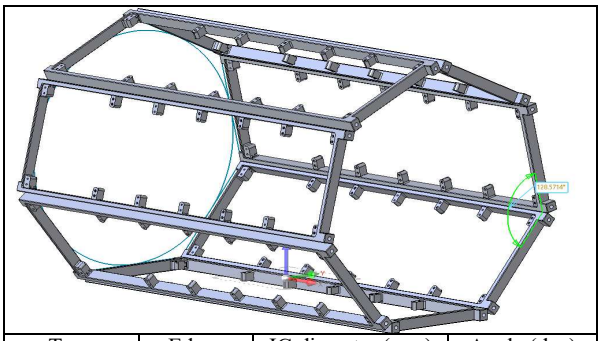

Type	Edges	IC diameter (mm)	Angle (deg)
Hepta	7	207.65	128.57

Fig. 6. Hepta unfolded.

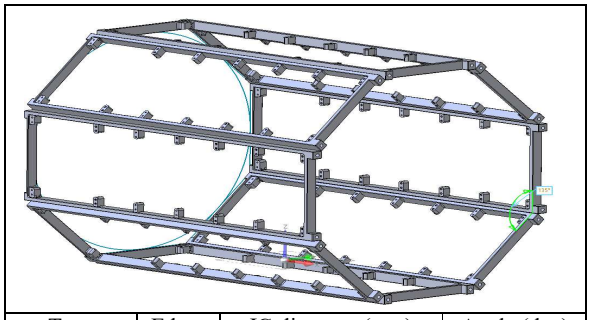

Type	Edges	IC diameter (mm)	Angle (deg)
Octa	8	241.42	135

Fig. 7. Octa unfolded.

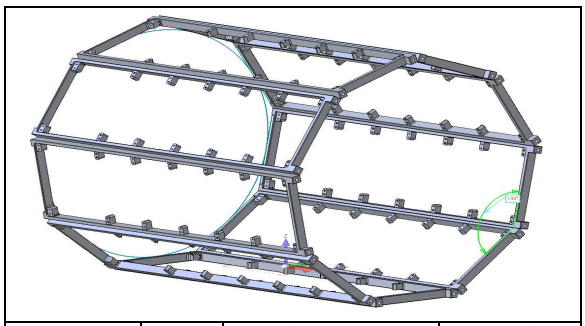

Type	Edges	IC diameter (mm)	Angle (deg)
Nona	9	274.75	140

Fig. 8. Nona unfolded.

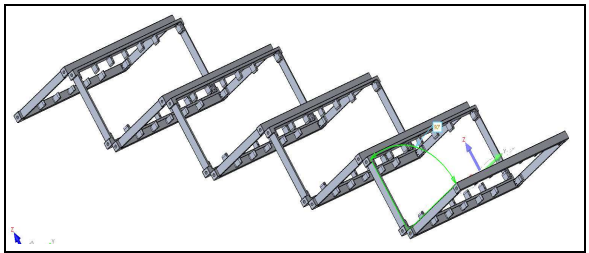

Type	Edges	IC diameter (mm)	Angle (deg)
Flip	2-9	-	90–180

Fig. 9. Flip unfolded.

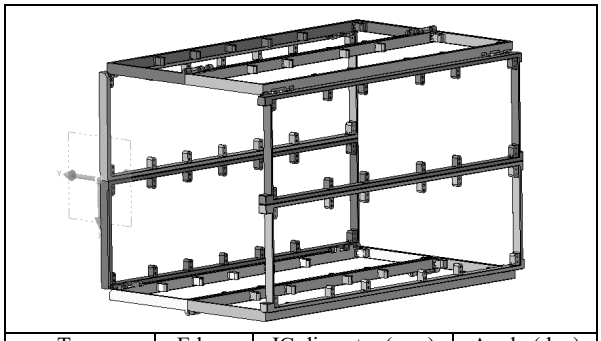

Type	Edges	IC diameter (mm)	Angle (deg)
QO-Cardsat	8	–	90–180

Fig. 10. QO-Cardsat unfolded.

Solar panels are mounted on the faces exposed to the Sun in the open configuration of Cardsat microsatellite.

In modeling and design, it is considered that the distance between two panels is ensured mechanically, either from the construction of the frame or with supporting elements.

The different distances between the panels may require constructive and/or dimensional solutions of different joints.

The axes of rotation of the joints will materialize halfway between two panels, alternately left-right, so that the folding of the panels is in the form of a closed fan.

It is considered that the opening of the panels is carried out simultaneously, at fixed angles, depending on the chosen configuration.

The configuration and size of the joints will be dictated by both the distance between the panels and the angle at which they will open.

Depending on the configuration and how the solar panels are mounted on the Cardsat frame, the number of joints of a certain type can vary between 3 and 4.

The actuation of the panels for opening is carried out with the help of springs [8, 10–17]:

- leaf springs;
- compression springs;
- torsion springs are a simple solution for opening two folding elements in a fixed position; torsion springs are dimensioned based on the maximum angles of rotation, the maximum force required to open and the maximum torque.

The materials for the springs must ensure the correct functioning of the assembly of which it is a part and be checked especially the expansion/contraction values due to variable temperatures within wide limits during 24 hours (−100 °C to +100 °C).

The testing of the operational functioning of the springs, within the corresponding assembly of the satellite of which they are a part, is done at the temperatures for which the basic structure of the satellite is also checked −40 °C to +85 °C.

Following the kinematic analyzes carried out for different configurations of Cardsat (quadri, penta, hexa, septa octa and nona, Figs. 3–8) and the identification of technical constraints - hinge-type joints with actuation by elastic elements of the lamellar spring type, spring of compression and torsion spring-the Quadro-Octo-Cardsat (Acronym QO-Cardsat) configuration from Fig. 10.

In the QO-Cardsat configuration the package consists of 8 Cardsat panels, with solar panels mounted on the faces exposed to the Sun in the open configuration. On each face, a solar panel protrudes 1 mm beyond the aluminum frame of the Cardsat panel structure. On the inner faces, the closing panels do not extend beyond the frame.

The width of the Cardsat panel is 100 mm.

The thickness of a frame is 10 mm.

It is noted that the first (frame no. 1) and the last (frame no. 8) aluminum frames have a special construction, with the ends designed in such a way as to allow ejection from the launcher. Thus, its length is 340.5 mm.

The intermediate frames (from no. 2 to no. 7) are of compact construction, with a length of 331 mm.

The imposed distance between two frames is:

- of 1.5 mm between faces with closing panels that do not exceed the height of the frame;
- of 4 mm between the faces on which the solar panels are mounted, so that the distance between the solar panels is 2 mm; a smaller distance may lead to panel damage due to launch conditions.

For the package of 8 panels, 3 joints between the frames with solar panels and 4 joints between the frames with simple panels were proposed in the design.

4. MATHEMATICAL MODEL PANEL POSITION CALCULUS FOR QO-CARDSAT

The following calculations are required to design the proposed QO-Cardsat configuration:

1. calculation of the opening of the QO-Cardsat configuration – determination of the angular positions of each opening joint of the panels so as to avoid possible collisions between the panels;
2. calculation of the torsion/lamination springs required for correct opening of the QO-Cardsat;
3. calculation of opening speeds.

For a correct calculation, the following assumptions were established:

- it is considered a symmetrical opening of the panels based on the principle of masses – in weightlessness conditions it is considered that if a reaction force acts between two bodies with different masses, then the body with the lower mass will move away from the body with the greater mass;
- for the calculation of the actuation of the QO-Cardsat panels, it is necessary to calculate the resistant moment on each joint generated by the mass of the panels set in motion.

For the calculation, it is considered that the most stressed joint is the middle joint, denoted by *C*0 according to Fig. 11.

The designed QO-Cardsat configuration is shown in Fig. 11 with overlapping panels and in Fig. 12 with the panels unfolded.

Joints are marked, in order, with *C*1, *C*2, *C*3, and symmetrical joints with *C*4, *C*5 and *C*6.

The following steps are taken:

1. coordinate systems are defined in each joint respecting the right hand rule;

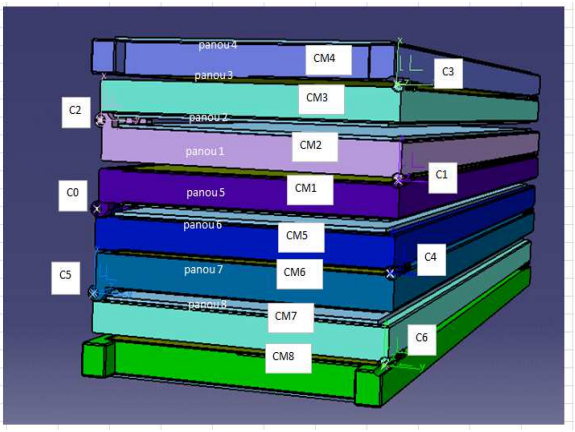

Fig. 11. QO-Cardsat folded package configuration.

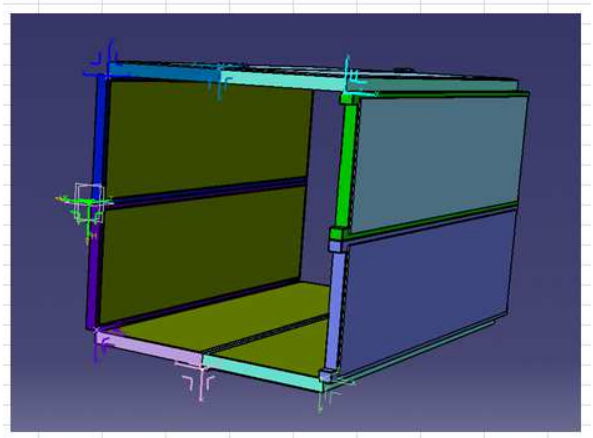

Fig. 12. QO-Cardsat configuration with panels deployed.

2. the positions of each joint are calculated according to the previous joints for each set angular position; this is how the position of each panel at a given moment is defined;
3. calculate the positions of each center of mass denoted by *CM*1, *CM*2, *CM*3, *CM*4 and, respectively, symmetrical centers of mass *CM*5, *CM*6, *CM*7, *CM*8;
4. calculate the resisting moment arm for each center of mass;
5. calculate the cumulative resistant moment on each joint according to the actuated panels;
6. the resisting moments thus calculated are used in the calculation of the springs required for the actuation.

4.1. Calculation of joint positions

The calculation of the joint positions is carried out with the help of rotation matrices.

Joint position 1 relative to joint 0 Rz0→1

$$ {}^{1}_{0}RT = {}^{1}_{0}R_z \cdot {}^{1}_{0}T_{xy} = $$
$$ = \begin{bmatrix} c\theta_0 & -s\theta_0 & 0 & 0 \\ s\theta_0 & c\theta_0 & 0 & 0 \\ 0 & 0 & 1 & 0 \\ 0 & 0 & 0 & 1 \end{bmatrix} \cdot \begin{bmatrix} 1 & 0 & 0 & lx_1 \\ 0 & 1 & 0 & ly_1 \\ 0 & 0 & 1 & 0 \\ 0 & 0 & 0 & 1 \end{bmatrix} \quad (1) $$

Joint position 2 relative to joint 0 Rz0→2

$$ {}^{2}_{0}RT = {}^{1}_{0}RT \cdot {}^{2}_{1}R_z \cdot {}^{2}_{1}T_{xy} = $$
$$ = {}^{1}_{0}RT \cdot \begin{bmatrix} c\theta_1 & -s\theta_1 & 0 & 0 \\ s\theta_1 & c\theta_1 & 0 & 0 \\ 0 & 0 & 1 & 0 \\ 0 & 0 & 0 & 1 \end{bmatrix} \cdot \begin{bmatrix} 1 & 0 & 0 & lx_2 \\ 0 & 1 & 0 & ly_2 \\ 0 & 0 & 1 & 0 \\ 0 & 0 & 0 & 1 \end{bmatrix} \quad (2) $$

Joint position 3 relative to joint 0 Rz0→3

$$ {}^{3}_{0}RT = {}^{2}_{0}RT \cdot {}^{3}_{2}R_z \cdot {}^{3}_{2}T_{xy} = $$
$$ = {}^{2}_{0}RT \cdot \begin{bmatrix} c\theta_2 & -s\theta_2 & 0 & 0 \\ s\theta_2 & c\theta_2 & 0 & 0 \\ 0 & 0 & 1 & 0 \\ 0 & 0 & 0 & 1 \end{bmatrix} \cdot \begin{bmatrix} 1 & 0 & 0 & lx_3 \\ 0 & 1 & 0 & ly_3 \\ 0 & 0 & 1 & 0 \\ 0 & 0 & 0 & 1 \end{bmatrix} \quad (3) $$

Joint position 4 relative to joint 0 Rz0→4

$$ {}^{4}_{0}RT = {}^{4}_{0}R_z \cdot {}^{4}_{0}T_{xy} = $$
$$ = \begin{bmatrix} c\theta_0 & -s\theta_0 & 0 & 0 \\ s\theta_0 & c\theta_0 & 0 & 0 \\ 0 & 0 & 1 & 0 \\ 0 & 0 & 0 & 1 \end{bmatrix} * \begin{bmatrix} 1 & 0 & 0 & lx_4 \\ 0 & 1 & 0 & ly_4 \\ 0 & 0 & 1 & 0 \\ 0 & 0 & 0 & 1 \end{bmatrix} \quad (4) $$

Joint position 5 relative to joint 0 *Rz*0 → 5

$$ {}^{5}_{0}RT = {}^{4}_{0}RT \cdot {}^{5}_{4}R_z \cdot {}^{5}_{4}T_{xy} = {}^{4}_{0}RT \cdot $$
$$ \cdot \begin{bmatrix} c\theta_4 & -s\theta_4 & 0 & 0 \\ s\theta_4 & c\theta_4 & 0 & 0 \\ 0 & 0 & 1 & 0 \\ 0 & 0 & 0 & 1 \end{bmatrix} \cdot \begin{bmatrix} 1 & 0 & 0 & lx_5 \\ 0 & 1 & 0 & ly_5 \\ 0 & 0 & 1 & 0 \\ 0 & 0 & 0 & 1 \end{bmatrix} \quad (5) $$

Joint position 6 relative to joint 0 *Rz*0 → 6

$$ {}^{6}_{0}RT = {}^{5}_{0}RT \cdot {}^{6}_{2}R_z \cdot {}^{6}_{2}T_{xy} = {}^{5}_{0}RT \cdot $$
$$ \cdot \begin{bmatrix} c\theta_5 & -s\theta_5 & 0 & 0 \\ s\theta_5 & c\theta_5 & 0 & 0 \\ 0 & 0 & 1 & 0 \\ 0 & 0 & 0 & 1 \end{bmatrix} \cdot \begin{bmatrix} 1 & 0 & 0 & lx_6 \\ 0 & 1 & 0 & ly_6 \\ 0 & 0 & 1 & 0 \\ 0 & 0 & 0 & 1 \end{bmatrix} \quad (6) $$

4.2. Calculation of the positions of the centers of mass

The calculation of the position of the centers of mass is carried out for each joint separately.

*CM*1 position relative to joint 0 *CM*0 → 0

$$ {}^{1}_{0}CM_1 = {}^{1}_{0}R_z \cdot {}^{1}_{0}T_{CM1} = $$
$$ = \begin{bmatrix} c\theta_0 & -s\theta_0 & 0 & 0 \\ s\theta_0 & c\theta_0 & 0 & 0 \\ 0 & 0 & 1 & 0 \\ 0 & 0 & 0 & 1 \end{bmatrix} \cdot \begin{bmatrix} 1 & 0 & 0 & Cx_1 \\ 0 & 1 & 0 & Cy_1 \\ 0 & 0 & 1 & 0 \\ 0 & 0 & 0 & 1 \end{bmatrix} \quad (7) $$

*CM*2 position relative to joint 0 *CM*2→0

$$ {}^{2}_{0}CM_2 = {}^{1}_{0}RT \cdot {}^{2}_{1}R_z \cdot {}^{2}_{1}T_{CM2} = {}^{1}_{0}RT \cdot $$
$$ \cdot \begin{bmatrix} c\theta_1 & -s\theta_1 & 0 & 0 \\ s\theta_1 & c\theta_1 & 0 & 0 \\ 0 & 0 & 1 & 0 \\ 0 & 0 & 0 & 1 \end{bmatrix} \begin{bmatrix} 1 & 0 & 0 & Cx_2 \\ 0 & 1 & 0 & Cy_2 \\ 0 & 0 & 1 & 0 \\ 0 & 0 & 0 & 1 \end{bmatrix} \quad (8) $$

*CM*3 position relative to joint 0 *CM*3 → 0

$$ {}^{3}_{0}CM_3 = {}^{2}_{0}RT \cdot {}^{3}_{2}R_z \cdot {}^{3}_{2}T_{CM2} = {}^{2}_{0}RT \cdot $$
$$ \cdot \begin{bmatrix} c\theta_2 & -s\theta_2 & 0 & 0 \\ s\theta_2 & c\theta_2 & 0 & 0 \\ 0 & 0 & 1 & 0 \\ 0 & 0 & 0 & 1 \end{bmatrix} \begin{bmatrix} 1 & 0 & 0 & Cx_3 \\ 0 & 1 & 0 & Cy_3 \\ 0 & 0 & 1 & 0 \\ 0 & 0 & 0 & 1 \end{bmatrix} \quad (9) $$

*CM*4 position relative to joint 0 *CM*4 → 0

$$ {}^{4}_{0}CM_4 = {}^{3}_{0}RT \cdot {}^{4}_{3}R_z \cdot {}^{3}_{2}T_{CM2} = {}^{3}_{0}RT \cdot $$
$$ \begin{bmatrix} c\theta_3 & -s\theta_3 & 0 & 0 \\ s\theta_3 & c\theta_3 & 0 & 0 \\ 0 & 0 & 1 & 0 \\ 0 & 0 & 0 & 1 \end{bmatrix} \cdot \begin{bmatrix} 1 & 0 & 0 & Cx_4 \\ 0 & 1 & 0 & Cy_4 \\ 0 & 0 & 1 & 0 \\ 0 & 0 & 0 & 1 \end{bmatrix} \quad (10) $$

*CM*2 position relative to joint 1 *CM*2 → 1

$$ {}^{2}_{1}CM_2 = {}^{2}_{1}R_z \cdot {}^{1}_{1}T_{CM2} = $$
$$ = \begin{bmatrix} c\theta_1 & -s\theta_1 & 0 & 0 \\ s\theta_1 & c\theta_1 & 0 & 0 \\ 0 & 0 & 1 & 0 \\ 0 & 0 & 0 & 1 \end{bmatrix} \cdot \begin{bmatrix} 1 & 0 & 0 & Cx_2 \\ 0 & 1 & 0 & Cy_2 \\ 0 & 0 & 1 & 0 \\ 0 & 0 & 0 & 1 \end{bmatrix} \quad (11) $$

*CM*3 position relative to joint 1 *CM*3 → 1

$$ {}^{3}_{1}CM_3 = {}^{2}_{1}RT \cdot {}^{3}_{2}R_z \cdot {}^{3}_{2}T_{CM3} = {}^{2}_{1}RT \cdot \begin{bmatrix} c\theta_2 & -s\theta_2 & 0 & 0 \\ s\theta_2 & c\theta_2 & 0 & 0 \\ 0 & 0 & 1 & 0 \\ 0 & 0 & 0 & 1 \end{bmatrix} \begin{bmatrix} 1 & 0 & 0 & Cx_3 \\ 0 & 1 & 0 & Cy_3 \\ 0 & 0 & 1 & 0 \\ 0 & 0 & 0 & 1 \end{bmatrix}. \quad (12) $$

*CM*4 position relative to joint 1 *CM*4 → 1

$$ {}^{4}_{1}CM_4 = {}^{3}_{1}RT \cdot {}^{4}_{3}R_z \cdot {}^{4}_{3}T_{CM4} = {}^{3}_{1}RT \cdot \begin{bmatrix} c\theta_3 & -s\theta_3 & 0 & 0 \\ s\theta_3 & c\theta_3 & 0 & 0 \\ 0 & 0 & 1 & 0 \\ 0 & 0 & 0 & 1 \end{bmatrix} \cdot \begin{bmatrix} 1 & 0 & 0 & Cx_4 \\ 0 & 1 & 0 & Cy_4 \\ 0 & 0 & 1 & 0 \\ 0 & 0 & 0 & 1 \end{bmatrix}. \quad (13) $$

*CM*3 position relative to joint 1 *CM*3 → 2

$$ {}^{3}_{2}CM_3 = {}^{3}_{2}R_z \cdot {}^{3}_{2}T_{CM3} = \begin{bmatrix} c\theta_2 & -s\theta_2 & 0 & 0 \\ s\theta_2 & c\theta_2 & 0 & 0 \\ 0 & 0 & 1 & 0 \\ 0 & 0 & 0 & 1 \end{bmatrix} \cdot \begin{bmatrix} 1 & 0 & 0 & Cx_3 \\ 0 & 1 & 0 & Cy_3 \\ 0 & 0 & 1 & 0 \\ 0 & 0 & 0 & 1 \end{bmatrix}. \quad (14) $$

*CM*4 position relative to joint 2 *CM*4 → 2

$$ {}^{4}_{2}CM_4 = {}^{3}_{2}RT \cdot {}^{4}_{3}R_z \cdot {}^{4}_{3}T_{CM4} = {}^{3}_{2}RT \cdot \begin{bmatrix} c\theta_3 & -s\theta_3 & 0 & 0 \\ s\theta_3 & c\theta_3 & 0 & 0 \\ 0 & 0 & 1 & 0 \\ 0 & 0 & 0 & 1 \end{bmatrix} \cdot \begin{bmatrix} 1 & 0 & 0 & Cx_4 \\ 0 & 1 & 0 & Cy_4 \\ 0 & 0 & 1 & 0 \\ 0 & 0 & 0 & 1 \end{bmatrix}. \quad (15) $$

*CM*4 position relative to joint 3 *CM*4 → 3

$$ {}^{4}_{3}CM_4 = {}^{4}_{3}R_z \cdot {}^{4}_{3}T_{CM4} = \begin{bmatrix} c\theta_3 & -s\theta_3 & 0 & 0 \\ s\theta_3 & c\theta_3 & 0 & 0 \\ 0 & 0 & 1 & 0 \\ 0 & 0 & 0 & 1 \end{bmatrix} \cdot \begin{bmatrix} 1 & 0 & 0 & Cx_4 \\ 0 & 1 & 0 & Cy_4 \\ 0 & 0 & 1 & 0 \\ 0 & 0 & 0 & 1 \end{bmatrix}. \quad (16) $$

4.3. Symmetrical panels

Position of *CM*5 relative to joint 0 *CM*5 → 0

$$ {}^{5}_{0}CM_5 = {}^{5}_{0}R_z \cdot {}^{5}_{0}T_{CM5} = \begin{bmatrix} c\theta_{0'} & -s\theta_{0'} & 0 & 0 \\ s\theta_{0'} & c\theta_{0'} & 0 & 0 \\ 0 & 0 & 1 & 0 \\ 0 & 0 & 0 & 1 \end{bmatrix} \cdot \begin{bmatrix} 1 & 0 & 0 & Cx_5 \\ 0 & 1 & 0 & Cy_5 \\ 0 & 0 & 1 & 0 \\ 0 & 0 & 0 & 1 \end{bmatrix}. \quad (17) $$

Position of *CM*6 relative to joint 0 *CM*6 → 0

$$ {}^{6}_{0}CM_6 = {}^{4}_{0}RT \cdot {}^{6}_{4}R_z \cdot {}^{6}_{4}T_{CM6} = {}^{4}_{0}RT \cdot \begin{bmatrix} c\theta_4 & -s\theta_4 & 0 & 0 \\ s\theta_4 & c\theta_4 & 0 & 0 \\ 0 & 0 & 1 & 0 \\ 0 & 0 & 0 & 1 \end{bmatrix} \cdot \begin{bmatrix} 1 & 0 & 0 & Cx_6 \\ 0 & 1 & 0 & Cy_6 \\ 0 & 0 & 1 & 0 \\ 0 & 0 & 0 & 1 \end{bmatrix}. \quad (18) $$

Position of *CM*7 relative to joint 0 *CM*7 → 0

$$ {}^{7}_{0}CM_7 = {}^{5}_{0}RT \cdot {}^{7}_{5}R_z \cdot {}^{7}_{5}T_{CM7} = {}^{5}_{0}RT \cdot \begin{bmatrix} c\theta_5 & -s\theta_5 & 0 & 0 \\ s\theta_5 & c\theta_5 & 0 & 0 \\ 0 & 0 & 1 & 0 \\ 0 & 0 & 0 & 1 \end{bmatrix} \cdot \begin{bmatrix} 1 & 0 & 0 & Cx_7 \\ 0 & 1 & 0 & Cy_7 \\ 0 & 0 & 1 & 0 \\ 0 & 0 & 0 & 1 \end{bmatrix}. \quad (19) $$

Position of *CM*8 relative to joint 0 *CM*8 → 0

$$ {}^{8}_{0}CM_8 = {}^{6}_{0}RT \cdot {}^{8}_{6}R_z \cdot {}^{8}_{6}T_{CM8} = {}^{8}_{0}RT \cdot \begin{bmatrix} c\theta_6 & -s\theta_6 & 0 & 0 \\ s\theta_6 & c\theta_6 & 0 & 0 \\ 0 & 0 & 1 & 0 \\ 0 & 0 & 0 & 1 \end{bmatrix} \cdot \begin{bmatrix} 1 & 0 & 0 & Cx_8 \\ 0 & 1 & 0 & Cy_8 \\ 0 & 0 & 1 & 0 \\ 0 & 0 & 0 & 1 \end{bmatrix}. \quad (20) $$

Position of *CM*6 relative to joint 4 *CM*6 → 4

$$ {}^{6}_{4}CM_6 = {}^{6}_{4}R_z \cdot {}^{6}_{4}T_{CM6} = \begin{bmatrix} c\theta_4 & -s\theta_4 & 0 & 0 \\ s\theta_4 & c\theta_4 & 0 & 0 \\ 0 & 0 & 1 & 0 \\ 0 & 0 & 0 & 1 \end{bmatrix} \cdot \begin{bmatrix} 1 & 0 & 0 & Cx_6 \\ 0 & 1 & 0 & Cy_6 \\ 0 & 0 & 1 & 0 \\ 0 & 0 & 0 & 1 \end{bmatrix}. \quad (21) $$

Position of *CM*7 relative to joint 4 *CM*7 → 4

$$ {}^{7}_{4}CM_7 = {}^{5}_{4}RT \cdot {}^{7}_{5}R_z \cdot {}^{7}_{5}T_{CM7} = {}^{5}_{4}RT \cdot \begin{bmatrix} c\theta_5 & -s\theta_5 & 0 & 0 \\ s\theta_5 & c\theta_5 & 0 & 0 \\ 0 & 0 & 1 & 0 \\ 0 & 0 & 0 & 1 \end{bmatrix} \cdot \begin{bmatrix} 1 & 0 & 0 & Cx_7 \\ 0 & 1 & 0 & Cy_7 \\ 0 & 0 & 1 & 0 \\ 0 & 0 & 0 & 1 \end{bmatrix}. \quad (22) $$

Position of *CM*8 relative to joint 4 *CM*8 → 4

$$ {}^{8}_{4}CM_8 = {}^{6}_{4}RT \cdot {}^{8}_{6}R_z \cdot {}^{8}_{6}T_{CM8} = {}^{6}_{4}RT \cdot \begin{bmatrix} c\theta_6 & -s\theta_6 & 0 & 0 \\ s\theta_6 & c\theta_6 & 0 & 0 \\ 0 & 0 & 1 & 0 \\ 0 & 0 & 0 & 1 \end{bmatrix} \cdot \begin{bmatrix} 1 & 0 & 0 & Cx_8 \\ 0 & 1 & 0 & Cy_8 \\ 0 & 0 & 1 & 0 \\ 0 & 0 & 0 & 1 \end{bmatrix}. \quad (23) $$

Position of *CM*7 relative to joint 5 *CM*7 → 5

$$ {}^{7}_{5}CM_7 = {}^{7}_{5}R_z \cdot {}^{7}_{5}T_{CM7} = \begin{bmatrix} c\theta_5 & -s\theta_5 & 0 & 0 \\ s\theta_5 & c\theta_5 & 0 & 0 \\ 0 & 0 & 1 & 0 \\ 0 & 0 & 0 & 1 \end{bmatrix} \cdot \begin{bmatrix} 1 & 0 & 0 & Cx_7 \\ 0 & 1 & 0 & Cy_7 \\ 0 & 0 & 1 & 0 \\ 0 & 0 & 0 & 1 \end{bmatrix}. \quad (24) $$

Position of *CM*8 relative to joint 5 *CM*8 → 5

$$ {}^{8}_{5}CM_8 = {}^{6}_{5}RT \cdot {}^{8}_{6}R_z \cdot {}^{8}_{6}T_{CM8} = {}^{3}_{2}RT \cdot \begin{bmatrix} c\theta_6 & -s\theta_6 & 0 & 0 \\ s\theta_6 & c\theta_6 & 0 & 0 \\ 0 & 0 & 1 & 0 \\ 0 & 0 & 0 & 1 \end{bmatrix} \cdot \begin{bmatrix} 1 & 0 & 0 & Cx_8 \\ 0 & 1 & 0 & Cy_8 \\ 0 & 0 & 1 & 0 \\ 0 & 0 & 0 & 1 \end{bmatrix}. \quad (25) $$

Position of *CM*8 relative to joint 0 6 *CM*8 → 6

$$ {}^{8}_{6}CM_8 = {}^{8}_{6}R_z \cdot {}^{8}_{6}T_{CM8} = \begin{bmatrix} c\theta_6 & -s\theta_6 & 0 & 0 \\ s\theta_6 & c\theta_6 & 0 & 0 \\ 0 & 0 & 1 & 0 \\ 0 & 0 & 0 & 1 \end{bmatrix} * \begin{bmatrix} 1 & 0 & 0 & Cx_8 \\ 0 & 1 & 0 & Cy_8 \\ 0 & 0 & 1 & 0 \\ 0 & 0 & 0 & 1 \end{bmatrix}. \quad (26) $$

where: ${}^{j}_{i}CM_j$ – the roto-translation matrix of the center of mass j with respect to the joint i; ${}^{j}_{i}RT$ – the roto-translation matrix of joint j with respect to joint i; ${}^{j}_{i}R_z$ – the z-axis rotation matrix of point j with respect to joint i where j is either the joint number or the center of mass number of the panel; ${}^{j}_{i}T_{CMj}$ – the translation matrix of the center of mass j with respect to the rotational couple i; ${}^{j}_{i}T_{xy}$ – the translation matrix of couple j with respect to the previous couple i with x and y coordinates.

A similar calculation is performed for symmetrical panels.

Once the position of the centers of mass relative to a given reference system is calculated, the moment arm of resistance is calculated with the Eq. (27):

$$bij = \sqrt{{}^{j}_{i}Cx^2 + {}^{j}_{i}Cy^2}, \quad (27)$$

where: ${}^{j}_{i}Cx$ – represents the position of the center of mass j with respect to the joint i in the x direction; ${}^{j}_{i}Cy$ – represents the position of the center of mass j with respect to the joint i direction y.

It is considered the gravitational acceleration g = 9.8 m/s^2 as the most unfavorable acceleration.

In space, the gravitational acceleration is variable according to Fig. 13.

The mass of a panel is estimated at the maximum m_j = 475 g, where j = 1–8.

The resisting moment on a coupler is given by the Eq. (28):

$$Mr_i = \sum_j^k F_j b_{ij} g, \quad (28)$$

where: i – joint number; j – mass center number (from 1 to 8); k – the maximum number of mass centers that have an effect on the calculated torque (4, 3, 2 or 1).

Resisting moments are used in the sizing of joint actuation springs.

5. RESULTS

The steps required for the technical design of the proposed panel configurations are those presented in detail in the design methodology:

1. kinematic calculation to identify the position of the panels and their centers of mass for given angles;
2. calculation of the resistant moments required to be overcome by the actuating elements of the spring type;
3. calculation of springs (torsion/lamination);
4. 3D modeling and detailing of QO-Cardsat panel assemblies;
5. verification by finite element analysis of the elaborated models.

The calculation methodology is implemented in an Excel application structured according to the scheme Figs. 11–12.

Based on the previous equations, load calculations were performed on each coupler depending on the relative position of the centers of mass.

An application was developed in which, depending on the dimensions of the structure and the estimation of the position of the center of mass on each panel, the resistant torsional moment in each coupler is automatically calculated.

Table 1 presents the main input data.

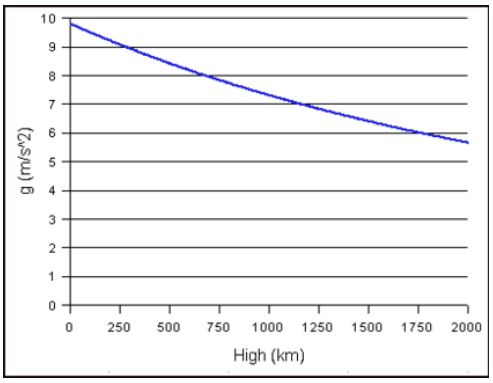

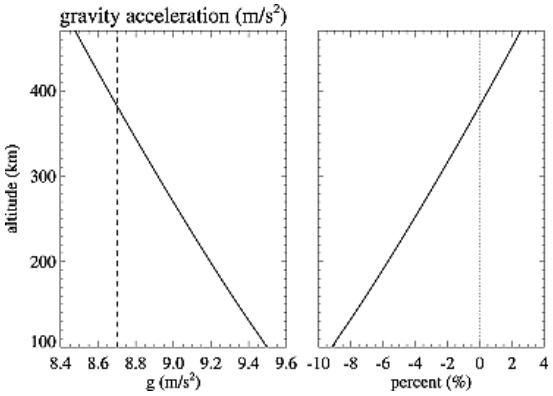

Fig. 13. Variation of gravitational acceleration g with altitude in space [18].

Table 1

Input data and preliminary calculations

Panels								
Panel	**1**	**2**	**3**	**4**	**5**	**6**	**7**	**8**
angle [deg]	-90	180	90	180	90	−180	−90	−180
angle [rad]	−1.57	3.14	1.57	3.14	1.57	−3.14	−1.57	−3.14
cos(angle)	0.00	−1	0.00	−1.00	0.00	-1.00	0.00	-1.00
sin(angle)	−1	0	1	0	1	−1.2E-16	-1	−1.2E-16
Joint position								
position X	0	12.75	12.75	12.75	0	−12.75	−12.75	−12.75
position Y	0	99.5	−99.5	98.5	0	98.5	−99.5	98.5
position Z	0	0	0	0	0	0	0	0
Position of mass centers per panel in coupler coordinates (can vary between 30 mm to 90 mm)								
Centers of mass	**CM1**	**CM2**	**CM3**	**CM4**	**CM5**	**CM6**	**CM7**	**CM8**
X [mm]	6.375	6.375	6.375	6.375	−6.375	−6.375	−6.375	−6.375
Y [mm]	49.25	−49.25	49.25	−49.25	49.25	−49.25	49.25	−49.25
Z [mm]	0	0	0	0	0	0	0	0
Loading force								
Mass [kg]	**0.3**	**0.475**	**0.475**	**0.3**	**0.475**	**0.475**	**0.475**	**0.475**
acceleration [m/s^2]	9	9.8	9.8	9.8	9.8	9.8	9.8	9.8
force [N]	2.7	4.655	4.655	2.94	4.655	4.655	4.655	4.655

Table 2
Joint coordinates in QO-Cardsat configuration

Joints positions	X	Y	Z
Joint 0	0	0	0
Joint 1	99.50	−12.75	0
Joint 2	112.25	112.25	0
Joint 3	−99.50	−11.75	0
Joint 4	−98.50	−12.75	0
Joint 5	−112.25	111.25	0
Joint 6	99.50	−12.75	0

Load joint 0

	Force arm [mm]	Force [N]	Torque Mt [Nmm]	
b01	49.66	2.7	134.08	Mt01
b02	122.69	4.655	571.13	Mt02
b03	100.39	4.655	467.32	Mt03
b04	185.80	2.94	546.25	Mt04
b05	49.66	4.655	231.17	Mt05
b06	121.83	4.655	567.12	Mt06
b07	100.02	4.655	465.61	Mt07
b08	52.83	4.655	245.94	Mt08
		Total	3228.63	

Load joint 1

	Force arm [mm]	Force [N]	Torque Mt [Nmm]	
b12	49.66	4.655	231.17	Mt12
b13	122.69	4.655	571.13	Mt13
b14	197.85	2.94	581.69	Mt14
		Total	1383.99	

Load joint 2

	Force arm [mm]	Force [N]	Torque Mt [Nmm]	
b23	49.66	4.655	231.17	Mt23
b24	99.09	2.94	291.33	Mt24
Total			522.50	

Load joint 3

	Force arm [mm]	Force [N]	Torque Mt [Nmm]	
b34	49.66	2.94	146.00	Mt23
		Total	146.00	

Load joint 4

	Force arm [mm]	Force [N]	Torque Mt [Nmm]	
b46	49.66	4.655	231.17	Mt12
b47	111.05	4.655	516.91	Mt13
b48	210.23	4.655	978.60	Mt14
Total			1726.69	

Load joint 5

	Force arm [mm]	Force [N]	Torque Mt [Nmm]	
b57	49.66	4.655	231.17	Mt23
b58	111.99	4.655	521.31	Mt24
		Total	752.48	

Load joint 6

	Force arm [mm]	Force [N]	Torque Mt [Nmm]	
b78	49.66	4.655	231.17	Mt23
		Total	231.17	

In the open configuration, the positions of the rotation axes relative to the reference system are calculated based on the homogeneous transformation equations. For simplification, coordinate systems are used in each joint with the same orientation of the *Z* axis (along the axis of rotation). The results are presented in Table 2.

The results are using for springs calculus used for opening the panels.

6. CONCLUSION

The studies presented in this article are the preliminary calculations necessary for the design of the actuation elements of Cardsat type panels, in combined construction.

Following the calculations, the passive actuation joints will be dimensioned to define specific type architectures QO-Cardsat.

Thus, a closed Cardsat structure can have a number of applications in the aerospace industry, practically transforming a simple microsatellite into a complex one.

Homogeneous transformation matrices were used for the calculation of resistant torsional moments, mass data of each panel in different positions starting from the closed configuration to the open configuration.

Once the equations were obtained, they were implemented in a software application to ensure the flexibility and dynamics of the calculation for different angular positions.

In the example presented, resistant torsional moments were calculated for the configuration with 8 panels in a sliding opening 90°, 180°, 90°, 180°–180°, 90°, 180°, 90°. Based on these calculations, the specific joints were dimensioned.

The next step consists in manufacturing a first prototype of QO-Cardsat and validating the concept through practical tests.

Acknowledgments: This research was carried out within the project: "Innovative technologies for the processing and testing of advanced aerospace materials", ID MySMIS 120353, financed by Competitiveness Operational Program POR Action 1.2.1.

REFERENCES

[1] A.K. Maini, V. Agrawal, *Satellite technology: principles and applications*, 2nd ed. John Wiley & Sons, 2011.

[2] T. Blachowicz, K. Pająk, P. Recha, A. Ehrmann, *3D printing for microsatellites-material requirements and recent developments*, AIMS Materials Science, vol. 7, no. 6, 2020, pp. 926–938.

[3] A. Ampatzoglou, V. Kostopoulos, *Design, Analysis, Optimization, Manufacturing, and Testing of a 2U Cubesat*, International Journal of Aerospace Engineering, Hindawi Volume 2018, 9724263, 2018.

[4] C. Cappelletti, S. Battistini, B.K. Malphrus, (Eds.), *CubeSat Handbook: From Mission Design to Operations*, Academic Press, Elsevier, 2021.

[5] A. Vricella, A. Delfini, M. Albano, F. Santoni, R. Pastore, G. Rubini, M. Marchetti, *Study and ground simulations of outgassing and hypervelocity impacts on carbon-based materials for space applications*, In 5th IEEE International Workshop on Metrology for AeroSpace (MetroAeroSpace), 2018, pp. 652–657.

[6] *** Project ADCOTMAT, Studiul materialelor compozite avansate, sisteme de acoperiri, definirea proceselor si cerintelor preliminare (*Study of advanced composite*

materials, coating systems, definition of processes and preliminary requirements), INCAS, 2013.
[7] M. Wu, T. Zhang, P. Xiang, F. Guan, *Single-layer deployable truss structure driven by elastic components*, Journal of Aerospace Engineering, vol. 32, no. 2, 2019, p. 04018144.
[8] I.A. Lomaka, N.A. Elisov, E. A. Boltov, S.V Shafran, *A novel design of CubeSat deployment system for transformable structures*, Acta Astronautica, 197, 2022, pp. 179–190.
[9] F. Abdullah, K.I. Okuyama, I. Fajardo, N. Urakami, *In situ measurement of carbon fibre/polyether ether ketone thermal expansion in low earth orbit*. Aerospace, vol. 7, no. 4, 2020, p. 35.
[10] P. Hohn, *Design, construction and validation of an articulated solar panel for CubeSats*, Master's Thesis, Lulea Tekniska Universitet, Lulea, 2010.
[11] A. Solís-Santomé, G. Urriolagoitia-Sosa, B. Romero-Ángeles, C.R. Torres-San Miguel, J.J. Hernández-Gómez, I. Medina-Sánchez, G. Urriolagoitia-Calderón, *Conceptual design and finite element method validation of a new type of self-locking hinge for deployable CubeSat solar panels*, Advances in Mechanical Engineering, vol. 11, no. 1, 2019, p. 1687814018823116.
[12] S. Morterolle, *Étude de structures légères déployables pour applications spatiales*, PhD Thesis, L'universite Montpellier 2, 2011.
[13] E. Picault, *Un modèle de poutre à section mince flexible - Application aux pliages 3D de mètres rubans*, PhD Thesis, Universite d'Aix-Marseille, 2013.
[14] F. Santoni et al. F. Piergentili, S. Donati, M. Perelli, A. Negri, M. Marino, *An innovative deployable solar panel system for Cubesats*, Acta Astronautica, vol. 95, 2014, pp. 210–217.
[15] J.W. Jeong, Y.I. Yoo, D.K. Shin, J.H. Lim, K.W. Kim, J.J. Lee, *A novel tape spring hinge mechanism for quasi-static deployment of a satellite deployable using shape memory alloy*, Review of Scientific Instruments, vol. 85, no. 2, 2014, p. 025001.
[16] D.Y. Kim, H.S. Choi, J.H. Lim, K.W. Kim, J. Jeong, *Experimental and numerical investigation of solar panels deployment with tape spring hinges having nonlinear hysteresis with friction compensation*, Applied Sciences, vol. 10, no. 21, 2020, p. 7902.
[17] T. Murphy, J. Kanaber, C. Koehler, *PEZ: expanding CubeSat capabilities through innovative mechanism design*, 25th Annual AIAA/USU Conference on Small Satellites, Logan, Utah, August, 2011, p. 4.
[18] Y. Deng, A.J. Ridley, W. Wang, *Effect of the altitudinal variation of the gravitational acceleration on the thermosphere simulation*, Journal of Geophysical Research: Space Physics, 113, A09302, 2008.
[19] E. Kulu, *Small Launchers – 2021 Industry Survey and Market Analysis*, 72nd International Astronautical Congress, Dubai, United Arab Emirates, 25–29 October 2021, p. 24.
[20] *** *Cubesat Design Specification*, San Luis Obispo: Cal Poly SLO, p. 12, 2020.
[21] *** ESA – Deep space CubeSats, 2021, https://www.esa.int/Safety_Security/Hera/Deep_space_CubeSats.
[22] The European Cooperation for Space Standardization, Stangard ECSS-Q-ST-70C Rev. 2 – *Materials, mechanical parts and processes*, 2019, ECSS-Q-ST-70C Rev.2 – Materials, mechanical parts and processes (15 October 2019) | European Cooperation for Space Standardization.